Physical Communication 54 (2022) 101843

Contents lists available at ScienceDirect

Physical Communication

journal homepage: www.elsevier.com/locate/phycom

Full length article

A 3D indoor positioning system based on common visible LEDs

G. Cossu *, E. Ciaramella

Scuola Superiore Sant'Anna, Via Moruzzi 1, Pisa, Italy

ARTICLE INFO

Article history:
Received 21 March 2022
Received in revised form 15 July 2022
Accepted 5 August 2022
Available online 17 August 2022

MSC:
00-01
99-00

Keywords:
Indoor navigation
Light Emitting Diodes
Visible light

ABSTRACT

We propose a realistic 3D positioning system for indoor navigation that exploits visible Light Emitting Diodes (LEDs), placed on the ceiling. A unique frequency tone is assigned to each lamp and modulates its intensity in periodic time slots. The Time Difference of Arrival (TDOA) is measured without the need of a synchronization system between the sources and the receiver, then it is used to accurately estimate the receiver position. We first describe the theoretical approach, then propose the model and characterize the possible sources of noise. Finally, we demonstrate the proof-of-concept of the proposed system by simulation of lightwave propagation. Namely, we assess its performance by using Montecarlo simulations in a common room and estimate the impact of the different implementation parameters on the accuracy of the proposed solution. We find that, in realistic conditions, the technique allows for centimeter precision. Pushing the device requirements, the precision can be further increased to a sub-centimeter accuracy.

1. Introduction

Indoor positioning is attracting a growing interest for indoor navigation and location awareness because of the well-known limitations of the Global Position System (GPS) in indoor. Various approaches were proposed and demonstrated for both communication and positioning using Radio Frequency (RF) waves, thanks to their pervasive availability in indoor. Several researches of indoor localization exploit WiFi [1,2], Radio-Frequency IDentification (RFID) [3,4], Bluetooth [5,6], Ultra Wide Band (UWB) [7] or other similar RF-based solutions. However, these techniques provide a limited position accuracy. As an example, WiFi has an accuracy of 1 m to 7 m and Bluetooth between 2 m to 5 m [8]. They also have constrains in all areas where RF cannot be used, e.g. because of the Electro-Magnetic Interference (EMI).

Recently, an alternative indoor localization approach is emerging, which leverages on optical waves [8–12]. Lightwave-based localization is based on visible or infrared waves and can be quite more precise (0.01 m to 0.35 m). Moreover, Visible Light Positioning (VLP) has two key benefits, i.e. its synergy with illumination and robustness to EMI.

Positioning systems can be classified by the technique or the physical parameters that they exploit to obtain the position, such as angle, distance, time, or signal strength. The various VLP techniques include Angle of Arrival (AOA), Time of Arrival (TOA), TDOA and Received Signal Strength Indication (RSSI) [13]. AOA is the angle calculated relative to two or more reference points. The calculation of the angle is used to estimate the position of the Transmitter (TX) [14]. Differently, TOA is a distance-based technique. It measures the Time of Flight (TOF), i.e., the time taken by the signal to arrive at the Receiver (RX) from a fixed TX [15,16]. TOA uses the absolute time, hence it requires a precise time synchronization between TX and RX. As the TOA, also the TDOA is a distance-based technique: it determines the relative position of a RX from the difference of time of arrival between electromagnetic (EM) waves from multiple reference points, thus involves multiple TXs [17–23]. Thus, the TDOA removes the strict requirement to know when the signal was transmitted. A completely different technique is based on the RSSI: it measures the power level of the received signal and uses it to estimate the distance between TX and RX, knowing the optical emission profile of the source [14,24–26]. The main drawback of this technique is that the received signal is strongly affected by multipath and shadowing, which are relevant in all usual environments. Beside Photo-Diodes (PDs), a camera can also be used as receiver in a VLP system. Given their characteristics, the camera can be seen as an AOA sensor [27–30]. VLP systems exploiting all these different techniques has been demonstrated in the past. Various surveys presented a direct comparison between them in [8–10,31].

VLP based on TDOA technique is also been proposed in [32], where the authors simulate a 2D position method exploiting local oscillators both at TX and RX, phase-detectors and Hilbert transforms. Although the results show a position detection with sub-centimeter accuracy, no realistic characterization is presented: the simulation was built out only with ideal parameters. Moreover, the system suffers from the harmonic distortions, since the frequencies are integer multiples of a fundamental frequency.

* Corresponding author.
E-mail address: giulio.cossu@santannapisa.it (G. Cossu).

https://doi.org/10.1016/j.phycom.2022.101843

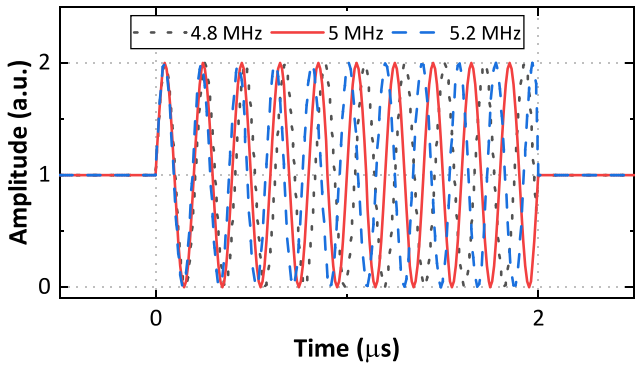

Fig. 1. Example of generated waveforms by the LEDs within a fixed (and common) time window. We assume three tones at 4.8, 5 and 5.2 MHz. The signals are within a 2 μs time window.

Here, we introduce and characterize a realistic 3D-VLP method. The proposed system exploits TDOA in such a way that it does not require signal synchronization between TX and RX, has no need of specific orientation of TX or RX and no need of a characterization of the optical power profile of the LEDs. It requires a minimum of 4 optical sources for a complete 3D positioning. The optical sources can be reduced to 3, if only a 2D positioning is required. The performance of the method are deeply characterized with realistic parameters and considering the sources of error of a practical implementation (SNR, multipath, ADC sampling rate, etc.). We include in our analysis the effectiveness of the system in case of a moving target.

The outline of the manuscript is the following: in Section 2, we introduce the proposed positioning method. In Section 3, we characterize the different sources of impairment of a practical implementation. In Section 4 we report the system performance evaluation varying the key system parameters. Finally, in Section 5, we draw the conclusion.

2. Proposed positioning method

We assume that a number of different white-light LED are placed at the ceiling; a minimum of 4 (3) sources are required for 3D (2D) VLP. Each LED emits an optical intensity that is modulated by a unique single frequency in a fixed (and common) time window of length T. As an example, we report in Fig. 1 the output intensity of three LEDs, where the tones are at 4.8, 5 and 5.2 MHz, respectively, and $T = 2$ μs. These frequency values are chosen as a possible real implementation: they are high enough to provide a good accuracy and, at the same time, are within the typical modulation bandwidth of the LEDs.

The RX detects the superimposition of the modulated signals, received with different amplitudes and TOF values, due to the individual optical paths. We can thus measure the TDOA of the different sources, derive the path length differences, and use them to calculate the target position.

Ideally, the received photo-current $s(t)$ contains only the overlap of the N tones with different TOF τ_j (where j is the index of the optical source):

$$s(t) = \sum_{j=0}^{N-1} a_j \sin\left(2\pi f_j (t - \tau_j)\right) \tag{1}$$

where N is the number of sources. Each τ_j is given by:

$$\begin{aligned}\tau_j &= R(x_j, y_j, z_j)/c \\ &= \sqrt{(x_j - X)^2 + (y_j - Y)^2 + (z_j - Z)^2}\Big/c\end{aligned} \tag{2}$$

where $[x_j, y_j, z_j]$ and $[X, Y, Z]$ are the coordinates of the jth LED and of the target, respectively; c is the speed of light.

The acquisition starts with arrival of the first (the closest) optical source signal. This implies that the tones from the optical sources are transmitted within the same time window to easily identify a starting point. Including this effect, Eq. (1) slightly changes to:

$$s(t) = \sum_{j=1}^{N} a_j \sin\left(2\pi f_j (t - \Delta\tau_{jo})\right) \tag{3}$$

where o is the index of the nearest source, which works as a trigger of the acquisition, and $\Delta\tau_{jo} = \tau_j - \tau_o$.

In order to extract the TDOA, we perform the Fourier Transform (FT), which separates the frequency components and their phases:

$$S(f_j) \equiv \mathcal{F}\left(s(t)_{f_j}\right) = \frac{i}{2}\left(\sum_{j=1}^{N} \delta(f \pm f_j) e^{2\pi f_j \Delta\tau_{jo}}\right) \tag{4}$$

where $\mathcal{F}(\cdot)$ indicates the FT operator and $\delta(\cdot)$ is Dirac function. The argument of $S(f_j)$ includes the information of the TDOA $\Delta\tau$ at a specific frequency:

$$\phi_j = 2\pi f_j \Delta\tau_{jo} = \arg(2iS(f_j)) \tag{5}$$

where arg is the argument of the complex number, which is defined as $\arg(z) = \arctan(\Im(z)/\Re(z))$. Hence, the $\Delta\tau_{jo}$ of a specific optical source j is given by

$$\Delta\tau_{jo} = \frac{\phi_j}{2\pi f_j} \tag{6}$$

The target coordinates $[X, Y, Z]$ can be estimated from the trilateration of the N $\Delta\tau$ values:

$$\begin{aligned}\Delta\tau_{jo} &= \left(R(x_j, y_j, z_j) - R(x_o, y_o, z_o)\right)/c \\ &= \sqrt{(x_j - X)^2 + (y_j - Y)^2 + (z_j - Z)^2}\Big/c \\ &- \sqrt{(x_o - X)^2 + (y_o - Y)^2 + (z_O - Z)^2}\Big/c\end{aligned} \tag{7}$$

which creates a system with 3 unknown values (the coordinates of the target) and $N - 1$ equations. Therefore, a minimum of 4 optical sources are required for a 3D positioning, since that one source is used for time reference and the other three for trilateration. Eq. (7) gives the difference of path distance divided by speed of light, which means the difference of arrival time from two sources. The subscript o indicates the optical signal used as reference, e.g., the signal that arrives first to the target (and is used as trigger for the acquisition). The subscript j indicates all the other signals, from which we compute the TDOA values and therefore the target position. j and o optical sources could be different depending on the location of the target.

The analytical solution of the intersection of generic hyperboloids exists only for particular sources positions, hence it is not considered here. Available solutions are the numerical or the approximate solution based on the linearization of the equations: Taylor series (truncated at the first order) [33,34] or Chan and Ho solution [35]. In the proposed method, we exploit the numerical solution to extract the target position $[X, Y, Z]$.

3. Noise characterization

Here, we characterize our method including the typical impairments in a realistic implementation. Let us consider an Additive White Gaussian Noise (AWGN) $n(t)$, with standard deviation σ_n, on the received signal $s(t)$. This is a good approximation for the thermal noise in common photodiodes. Clearly, this noise

has an impact on the amplitude and the phase of the complex value of the Fast Fourier Transform (FFT) $S(f_j)$. However, the proposed positioning method is sensitive only to the phase of FFT components, whose standard deviation can be estimated using the common error propagation formula:

$$\sigma_\phi = \frac{\partial \phi}{\partial n}\sigma_n = \frac{\sigma_n}{|S(f_j)|} \tag{8}$$

This implies that the phase error is proportional to the standard deviation of the AWGN noise and decreases with the signal amplitude. This means that the phase noise is inversely proportional to the square root of the SNR:

$$\sigma_\phi \propto \frac{1}{\sqrt{\text{SNR}}} \tag{9}$$

Moreover, the SNR is proportional to the time window T, then $\sigma_\phi \propto 1/\sqrt{T}$. Finally, exploiting Eqs. (6) and (7), we can estimate the analytical trend of the accuracy, as a function of SNR, frequencies of the tones and time window:

$$\sigma_{[X,Y,Z]} \propto \frac{1}{f\sqrt{SNR}} \propto \frac{1}{f\sqrt{T}} \tag{10}$$

We conclude that we can improve the accuracy if we increase the frequency tones and the time window.

3.1. Multipath

The multipath effect has a strong impact on all localization techniques [36]. Therefore, we modeled the effect of the multipath in our case, which produces an overlap of the Line-of-Sight (LOS) waves with other attenuated waves (from reflections) with same frequency f, amplitudes a_k and delays $\Delta\tau_k$.

$$S(f) \propto a_0 e^{2\pi i f \Delta\tau_0} + \sum_{k=1}^{M} a_k e^{2\pi i f \Delta\tau_k} \tag{11}$$

where the subscripts 0 indicates the LOS components and M are the relevant multiple paths. Since that $\Delta\tau$ is in the order of ns and $2\pi f \Delta\tau \sim 10^{-2} \ll 1$, we can exploit the approximation for small numbers:

$$\phi = \arg(2iS(f)) \sim \left(\frac{a_0 2\pi f \Delta\tau_0 + \sum a_k 2\pi f \Delta\tau_k}{a_0 + \sum a_k}\right) \tag{12}$$

Hence, the estimated TDOA value $\overline{\Delta\tau}$ is given by

$$\overline{\Delta\tau} = \frac{\Delta\tau_0 + \sum a_k/a_0 \Delta\tau_k}{1 + \sum a_k/a_0} \tag{13}$$

which results in an overestimation of the LOS value and depends on the delays and amplitudes of the reflections. As can be noted, in absence of reflections ($a_k = 0$) $\overline{\Delta\tau} = \Delta\tau_0$. The impact of the multipath on the system performance is estimated in Section 4.

3.2. Synchronization

When describing the model, we assumed to have synchronous sources, but no synchronization between TX and RX. It may seem a strong assumption, but it can be effectively handled. A first solution could be to generate different tones using a single oscillator and then exploit a frequency multiplier. However, this solution may be still affected by the fact that other delays can arise also in this configuration (path delay), and could generate harmonic distortions, reducing the position accuracy. On the other side, we can imaging to calibrate the system once, placing the target in a known position and measuring the TDOA from the different sources. As an example, the target can be placed at the center of the room, hence the same $\Delta\tau$ should be measured from all sources, in principle. When a different value is measured, the phase of the sinewave used to modulate that optical source can be adjusted to compensate the time mismatches.

Table 1
Default parameters used for the simulations.

Default parameters	Values
Number of optical sources	4
Ceiling height	3 m
Target coordinates	(0,0,0) m
Sources coordinates	(−2,-2,3), (−2,2,3), (2,−2,3), (2,2,3) m
Time window	1 ms
Sampling rate	20 MSa/s
Average tone's frequency	5 MHz
SNR	20 dB
Bit vertical resolution	10 bits
Phase noise	0 rad
Multipath	0 reflections

4. Performance evaluation

In order to assess the performance of the proposed positioning architecture, we modeled the light propagation in a room; we varied the key independent parameters that can affect the accuracy of the VLP method and for each condition we performed Montecarlo simulations. All the simulations results were performed implementing the described formulas in MATLAB. In Table 1, we report the list of parameters used in the simulations and their values.

In Fig. 2, we depict the simulation environment. It is a 6 × 6 × 3 m room, where 4 LEDs are at the ceiling at the corners of a square with 4 m sides. The tones are separated by 100 kHz and centered at 5 MHz.

We generated the signal $s(t_k)$ as superimposition of tones with different arrival phases depending on the real distance from the target. This is modeled to include the noise, the multipath, and the quantization of time and amplitude, etc. The multipath effect was introduced by adding a series of tones at the same frequency attenuated compared to the LOS term and with longer TOF, as in [37], from which the amplitude and delay values were taken. $s(t_k)$ emulates the expected received optical signals detected by a photodiode a eventually acquired by means of a ADC.

Then, we apply the algorithm described in section Section 2, which first computes the FFT to extract the phase and time of arrival information (Eqs. (5) and (6)), and then estimates the $[\bar{X}, \bar{Y}, \bar{Z}]$ target position, solving Eq. (7) by a numerical solution. To calculate the position accuracy, we computed the error vector between the target point and the estimated one, as in the following for 3D and 2D accuracy, respectively:

$$d_{XYZ} = \sqrt{(X-\bar{X})^2 + (Y-\bar{Y})^2 + (Z-\bar{Z})^2} \tag{14}$$

$$d_{XY} = \sqrt{(X-\bar{X})^2 + (Y-\bar{Y})^2} \tag{15}$$

In each condition, the simulation was iterated 500 times so that we can also have a statistical insight of the precision and estimate the variance of the obtained position value. The variance was introduced by the randomness of the AWGN and the multipath effect of the received lightwave.

4.1. Simulation results

In Fig. 3, we report the estimated VLP accuracy at every position of the floor, with two different configurations of the optical sources, namely a square or triangle arrangements. The accuracy in the two configurations is similar. In the first case, the accuracy has a smooth trend for the different positions. In the second configuration, the system has higher precision at the center and lower at the corner than in the previous case. As we see, in most

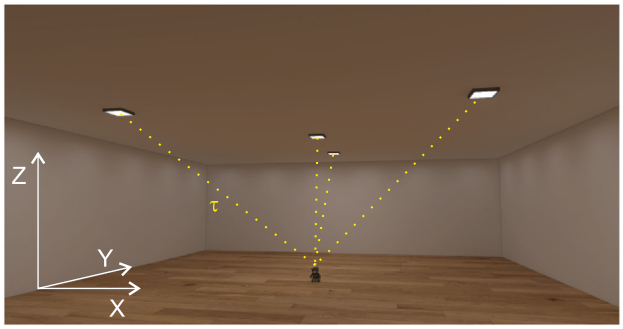

Fig. 2. Schematic representation of the room scenario adopted in the simulations.

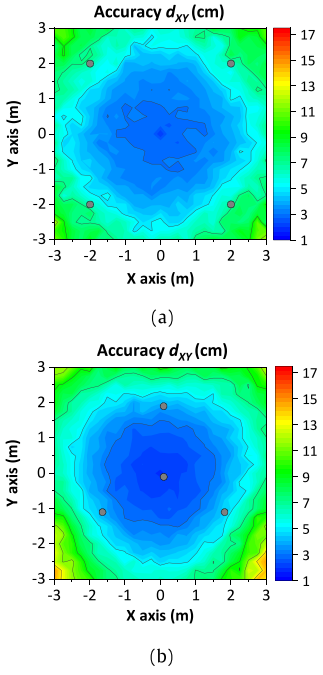

Fig. 3. Estimated 2D system accuracy of the proposed model over a $6 \times 6\,m^2$ area for a square (a) and triangle (b) shape position of the optical source. The gray dots indicate the position of the optical sources at the ceiling within the simulated room. Colorbars on the right indicate the accuracy scale.

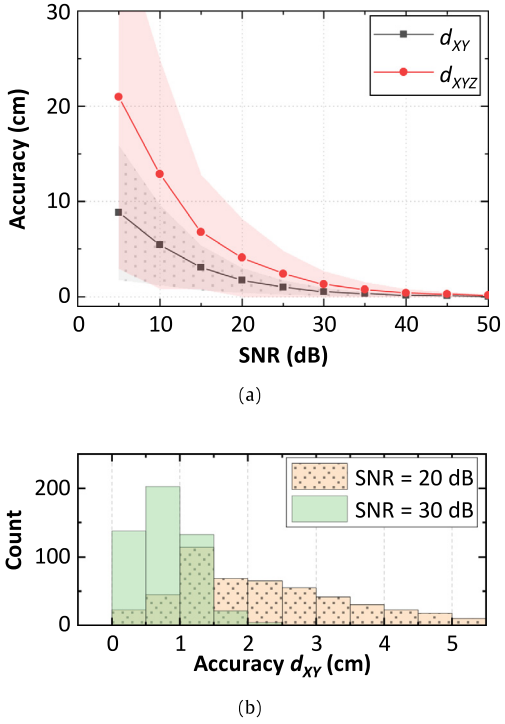

Fig. 4. (a) Position accuracy for 3D and 2D system as a function of the SNR of the received signal. The semi-transparent colored areas indicate the standard variations of the corresponding accuracy estimations As expected, it is strongly reduced at high SNR. (b) Accuracy distribution at 20 and 30 dB of SNR.

of the room (± 2 m) the accuracy is better than 5 cm. Only at the room corners (± 3 m), the error increases up to $7-12$ cm. The position accuracy is higher in the area defined by the optical source positions ($16\,m^2$). As mentioned above, these results are obtained using the parameters reported in Table 1.

In Fig. 4(a), we report the accuracy for 2D and 3D positioning as a function of the SNR of the received signal. As expected, the accuracy improves at higher SNR and well fits the analytic model expressed in Eq. (10), which states that the error reduces with the inverse of the square root of the SNR (in linear scale). At SNR$>$30 dB, the positioning system reaches sub-centimeter accuracy. This condition is not hard to be achieved considering the intensity of the light used for illumination and the modulation power all concentrated in a single tone.

We highlight that the system provides a better accuracy if we consider only 2D positioning. Since the sources are placed on the same plane (the ceiling), we observed a higher error on Z-axis compared to X- and Y-axis.

The semi-transparent colored areas indicate the standard variations of the corresponding accuracy estimations. As expected, the variation strongly reduced at high SNR. As an example, we report the accuracy distribution over 500 simulations in Fig. 4(b), for SNR $=$ 20 dB and SNR $=$ 30 dB.

A similar trend is reported in Fig. 5, where we present the position accuracy as a function of the time window T. Also for this parameter, the trend follows the model described in Section 3: the position accuracy scales with the inverse of the square root of T. Increasing T to values > 0.1 s, we can obtain sub-centimeter accuracy (considering the default value of SNR$=$ 20 dB), for a static target. This accuracy can reduce if the target is moving because non-static targets cannot benefit completely from a long time window. In Fig. 6, we report the accuracy d_{XY} as a function of the target speed (from 1 m/s to 4 m/s) along a specific X-axis, for $T = 1$ ms and $T = 10$ ms.

As expected, when we have a short time window ($T = 1$ ms), the distance covered by the target ($\sim$ mm) is lower then the position accuracy (in the order of cm), hence no appreciable variation is noted. On the other hand, when using wider time windows ($T = 10$ ms), the accuracy reduces with the distance covered by

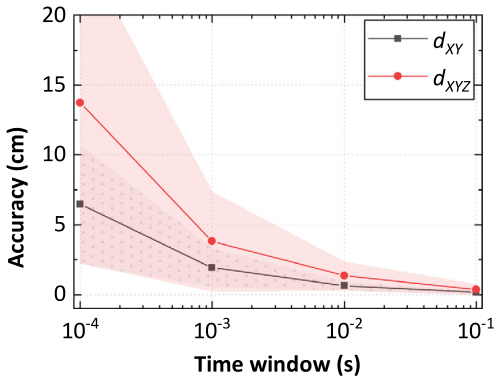

Fig. 5. Position accuracy for 3D and 2D system as a function of the waveform time window. The semi-transparent colored areas indicate the standard variations of the corresponding accuracy estimations.

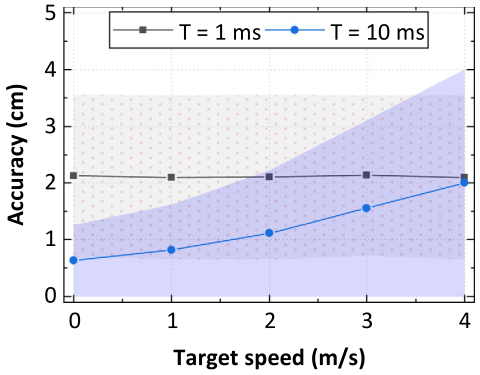

Fig. 6. Position accuracy as a function of the speed of a moving target along X-axis, for two different time window length. The semi-transparent colored areas indicate the standard variations of the corresponding accuracy estimations.

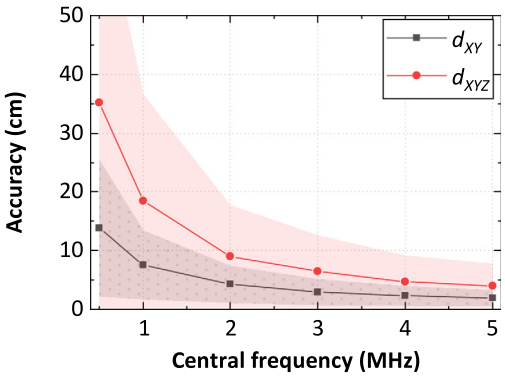

Fig. 7. Position accuracy for 3D and 2D system as a function of the central frequency of the tones used to identify the optical sources. The semi-transparent colored areas indicates the standard variation of the corresponding accuracy estimation.

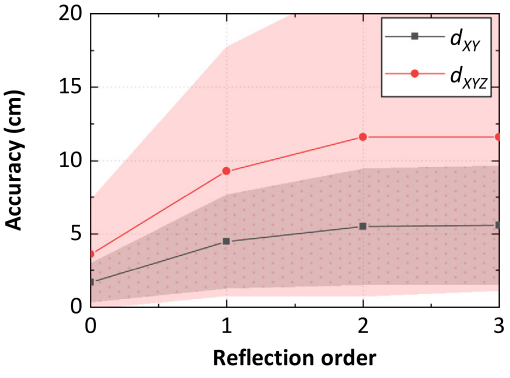

Fig. 8. Position accuracy for 3D and 2D system as a function of the order of reflection from an object in the room considered in the simulation. The semi-transparent colored areas indicate the standard variations of the corresponding accuracy estimations.

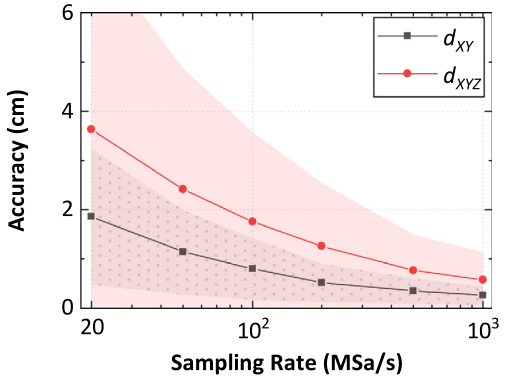

Fig. 9. Position accuracy fro 3D and 2D configuration as a function of the ADC sampling rate. The semi-transparent colored areas indicate the standard variations of the corresponding accuracy estimations.

the target within the time T, since it becomes compatible with the position accuracy. However, the accuracy is still better than the previous case, with shorter time window (considering realistic target speeds ≤ 16 km/s).

Other important parameter is the central frequency of the tones, reported in Fig. 7. In this case, the theory suggests that the accuracy improves when increasing the frequency. Using low frequency tones, the position accuracy gets worse; as an example, it can be > 30 cm at 500 kHz.

In Fig. 8, we report the effect of the multipath in the positioning system. Clearly, the reflections have a strong impact on the accuracy since they influence directly the estimation of the time of arrival. From the results, we note that the position accuracy is mostly determine by the first 2 reflections, since the 3rd reflection is typically too small to have effects.

We ended up analyzing the effects of the horizontal (time) and vertical (amplitude) quantization of the received signal by means of a real ADC. The results of the accuracy as a function of the sampling rate are reported in Fig. 9. As expected, increasing the sampling rate, the integrity of the sampled signal is higher, therefore also the accuracy of the estimated position improves. Passing from 20 MSa/s to 1 GSa/s, the accuracy improves from 4 to 0.5 cm, in 3D positioning configuration.

A different behavior is reported in Fig. 10, where we report the position accuracy as a function of the vertical resolution of the ADC. The vertical resolution is expressed as the number of bits required to represent the different amplitude levels. In the simulation, we varied the amplitude quantization between 6 and 32 bits.

As can be seen, the signal is correctly received with 10 bits of ADC. An higher vertical resolution no longer improves the positioning accuracy. ADCs with 10 bits in the required range of frequencies are quite common and cost-effective.

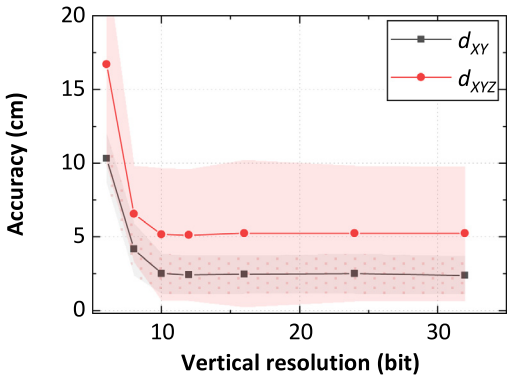

Fig. 10. Position accuracy fro 3D and 2D configuration as a function of the vertical resolution of the ADC expressed in terms of number of bit.

5. Conclusion

We presented a realistic 3D VLP system and its detailed theoretical model. The proposed model is based on TDOA scheme that has no need for a precise synchronization between the optical sources and the receiver. In order to verify the performance of our method, we performed Montecarlo simulations that indicate a centimeter accuracy in a $6 \times 6\,m^2$ area. We also validated the model performing the simulations varying some practical parameters that must be take into account in a realistic implementation: received SNR, time window, target dynamic displacement, frequency of the tones, characteristics of the ADC, and multipath effect. The simulations are in agreement with the model.

Declaration of competing interest

The authors declare that they have no known competing financial interests or personal relationships that could have appeared to influence the work reported in this paper.

Data availability

No data was used for the research described in the article.

Acknowledgments

This article/publication is based upon work from COST Action CA19111, supported by COST (European Cooperation in Science and Technology).

References

[1] A. Zayets, E. Steinbach, Robust WiFi-based indoor localization using multipath component analysis, in: 2017 International Conference on Indoor Positioning and Indoor Navigation (IPIN), IEEE, Sapporo, Japan, 2017, pp. 1–8, http://dx.doi.org/10.1109/IPIN.2017.8115943.

[2] C. Chen, Y. Han, Y. Chen, K.J.R. Liu, Indoor GPS with centimeter accuracy using WiFi, in: 2016 Asia-Pacific Signal and Information Processing Association Annual Summit and Conference (APSIPA), IEEE, Jeju, Korea (South), 2016, pp. 1–4, http://dx.doi.org/10.1109/APSIPA.2016.7820842.

[3] X. Chen, Z.J. Wang, Reliable indoor location sensing technique using active RFID, in: 2010 the 2nd International Conference on Industrial Mechatronics and Automation, Vol. 1, IEEE, Wuhan, China, 2010, pp. 160–163, http://dx.doi.org/10.1109/ICINDMA.2010.5538059.

[4] X. Jiang, Y. Liu, X. Wang, An enhanced approach of indoor location sensing using active RFID, in: 2009 WASE International Conference on Information Engineering, Vol. 1, IEEE, Taiyuan, China, 2009, pp. 169–172, http://dx.doi.org/10.1109/ICIE.2009.204.

[5] J. Schmalenstroeer, R. Haeb-Umbach, Investigations into Bluetooth low energy localization precision limits, 2016, http://dx.doi.org/10.1109/eusipco.2016.7760329.

[6] K. Mundnich, B. Girault, S. Narayanan, Bluetooth based indoor localization using triplet embeddings, 2019, http://dx.doi.org/10.1109/icassp.2019.8683715.

[7] M.R. Gholami, E.G. Ström, F. Sottile, D. Dardari, A. Conti, S. Gezici, M. Rydström, M.A. Spirito, Static positioning using UWB range measurements, in: 2010 Future Network & Mobile Summit, IEEE, Florence, Italy, 2010, pp. 1–10.

[8] N.U. Hassan, A. Naeem, M.A. Pasha, T. Jadoon, C. Yuen, Indoor positioning using visible LED lights: A survey, ACM Comput. Surv. (2015) 1–32, http://dx.doi.org/10.1145/2835376.

[9] A.B.M.M. Rahman, T. Li, Y. Wang, Recent advances in indoor localization via visible lights: A survey, Sensors 20 (5) (2020) http://dx.doi.org/10.3390/s20051382.

[10] Y. Zhuang, L. Hua, L. Qi, J. Yang, P. Cao, Y. Cao, Y. Wu, J. Thompson, H. Haas, A survey of positioning systems using visible LED lights, IEEE Commun. Surv. Tutor. 20 (3) (2018) 1963–1988, http://dx.doi.org/10.1109/COMST.2018.2806558.

[11] C. Xie, W. Guan, Y. Wu, L. Fang, Y. Cai, The LED-ID detection and recognition method based on visible light positioning using proximity method, IEEE Photonics J. 10 (2) (2018) 1–16, http://dx.doi.org/10.1109/JPHOT.2018.2809731.

[12] W. Guan, S. Chen, S. Wen, Z. Tan, H. Song, W. Hou, High-accuracy robot indoor localization scheme based on robot operating system using visible light positioning, IEEE Photonics J. 12 (2) (2020) 1–16, http://dx.doi.org/10.1109/JPHOT.2020.2981485.

[13] F. Alkhawaja, M. Jaradat, L. Romdhane, Techniques of indoor positioning systems (IPS): A survey, in: 2019 Advances in Science and Engineering Technology International Conferences (ASET), 2019, pp. 1–8, http://dx.doi.org/10.1109/ICASET.2019.8714291.

[14] G.B. Prince, T.D. Little, Latency constrained device positioning using a visible light communication two-phase received signal strength-angle of arrival algorithm, in: 2015 International Conference on Indoor Positioning and Indoor Navigation (IPIN), IEEE, 2015, pp. 1–7.

[15] H.-X. Zhao, J.-T. Wang, A novel three-dimensional algorithm based on practical indoor visible light positioning, IEEE Photonics J. 11 (3) (2019) 1–8, http://dx.doi.org/10.1109/JPHOT.2019.2911738.

[16] Y. Zhang, H. Chen, S. Chen, J. Jin, Surface centroid TOA location algorithm for VLC system, KSII Trans. Internet Inf. Syst. (TIIS) 13 (1) (2019) 277–290.

[17] P. Du, S. Zhang, C. Chen, A. Alphones, W.-D. Zhong, Demonstration of a low-complexity indoor visible light positioning system using an enhanced TDOA scheme, IEEE Photonics J. 10 (4) (2018) 1–10, http://dx.doi.org/10.1109/JPHOT.2018.2841831.

[18] S.M. Sheikh, H.M. Asif, K. Raahemifar, F. Al-Turjman, Time difference of arrival based indoor positioning system using visible light communication, IEEE Access 9 (2021) 52113–52124.

[19] T.-H. Do, J. Hwang, M. Yoo, TDoA based indoor visible light positioning systems, in: 2013 Fifth International Conference on Ubiquitous and Future Networks (ICUFN), 2013, pp. 456–458, http://dx.doi.org/10.1109/ICUFN.2013.6614860.

[20] A. Naeem, N.U. Hassan, M.A. Pasha, C. Yuen, A. Sikora, Performance analysis of TDOA-based indoor positioning systems using visible LED lights, in: 2018 IEEE 4th International Symposium on Wireless Systems Within the International Conferences on Intelligent Data Acquisition and Advanced Computing Systems (IDAACS-SWS), 2018, pp. 103–107, http://dx.doi.org/10.1109/IDAACS-SWS.2018.8525567.

[21] E. Kazikli, S. Gezici, Hybrid TDOA/RSS based localization for visible light systems, Digit. Signal Process. 86 (2019) 19–28, http://dx.doi.org/10.1016/j.dsp.2018.12.001.

[22] C. Zhang, D. Li, X. Feng, L. Tan, L. Yang, X. Yang, Indoor visible light positioning method based on TDOA and fingerprint, in: 2021 IEEE International Conference on Electronic Technology, Communication and Information (ICETCI), 2021, pp. 397–401, http://dx.doi.org/10.1109/ICETCI53161.2021.9563479.

[23] Q. Hu, Y. Peng, Q. Wan, Z. Hu, Z. Wang, Y. Zhu, A novel 3-D localization scheme using 1-D AOA and TDOA measurements, in: 2021 IEEE 94th Vehicular Technology Conference (VTC2021-Fall), 2021, pp. 1–5, http://dx.doi.org/10.1109/VTC2021-Fall52928.2021.9625269.

[24] K. Wang, Y. Liu, Z. Hong, RSS-based visible light positioning based on channel state information, Opt. Express 30 (4) (2022) 5683–5699, http://dx.doi.org/10.1364/OE.451209.

[25] H. Steendam, T.Q. Wang, J. Armstrong, Theoretical lower bound for indoor visible light positioning using received signal strength measurements and an aperture-based receiver, J. Lightwave Technol. 35 (2) (2017) 309–319, http://dx.doi.org/10.1109/JLT.2016.2645603.

[26] B. Lin, X. Tang, Z. Ghassemlooy, C. Lin, Y. Li, Experimental demonstration of an indoor VLC positioning system based on OFDMA, IEEE Photonics J. 9 (2) (2017) 1–9, http://dx.doi.org/10.1109/JPHOT.2017.2672038.

[27] K. Aalimahmoodi, A. Gholami, Z. Ghassemlooy, An image sensor based indoor vlp system, in: 2018 9th International Symposium on Telecommunications (IST), IEEE, 2018, pp. 371–374.

[28] N.Q. Pham, K.A. Mekonnen, E. Tangdiongga, A. Mefleh, A.M.J. Koonen, Accurate indoor localization for beam-steered OWC system using optical camera, in: 45th European Conference on Optical Communication (ECOC 2019), 2019, pp. 1–4, http://dx.doi.org/10.1049/cp.2019.1079.
[29] J. Xu, C. Gong, Z. Xu, Experimental indoor visible light positioning systems with centimeter accuracy based on a commercial smartphone camera, IEEE Photonics J. 10 (6) (2018) 1–17, http://dx.doi.org/10.1109/JPHOT.2018.2878532.
[30] H. Cheng, C. Xiao, Y. Ji, J. Ni, T. Wang, A single LED visible light positioning system based on geometric features and CMOS camera, IEEE Photonics Technol. Lett. 32 (17) (2020) 1097–1100, http://dx.doi.org/10.1109/LPT.2020.3012476.
[31] G.B. Prince, T.D.C. Little, Two-phase framework for indoor positioning systems using visible light, Sensors 18 (6) (2018) http://dx.doi.org/10.3390/s18061917.
[32] S.-Y. Jung, S. Hann, C.-S. Park, TDOA-based optical wireless indoor localization using LED ceiling lamps, IEEE Trans. Consum. Electron. 57 (4) (2011) 1592–1597, http://dx.doi.org/10.1109/TCE.2011.6131130.
[33] J. Díez-González, R. Álvarez, L. Sánchez-González, L. Fernández-Robles, H. Pérez, M. Castejón-Limas, 3D TDOA problem solution with four receiving nodes, Sensors 19 (13) (2019) 2892.
[34] W.H. Foy, Position-location solutions by Taylor-series estimation, IEEE Trans. Aerosp. Electron. Syst. (2) (1976) 187–194.
[35] Y.-T. Chan, K. Ho, A simple and efficient estimator for hyperbolic location, IEEE Trans. Signal Process. 42 (8) (1994) 1905–1915.
[36] W. Gu, M. Aminikashani, P. Deng, M. Kavehrad, Impact of multipath reflections on the performance of indoor visible light positioning systems, J. Lightwave Technol. 34 (10) (2016) 2578–2587, http://dx.doi.org/10.1109/JLT.2016.2541659.
[37] J. Barry, J. Kahn, W. Krause, E. Lee, D. Messerschmitt, Simulation of multipath impulse response for indoor wireless optical channels, IEEE J. Sel. Areas Commun. 11 (3) (1993) 367–379, http://dx.doi.org/10.1109/49.219552.

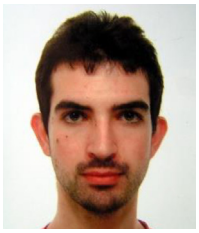

Giulio Cossu received M.S. degree in physics from University of Pisa (Italy) in 2010. He obtained his Ph.D. degree in 2014 at Scuola Superiore Sant'Anna (SA) of Pisa. Currently, he is Assistant Professor at SA. The main topic of his thesis was the investigation of innovative solutions of Optical Wireless Communications (OWC). His research interests include the areas of optical propagation through atmosphere, optical characterization, and optical communication. He was scientific responsible/technical officer for SA of the project "HYDRON PhaseA" and "HYDRON Simulation TestBed", both founded by ESA. He is in the workgroup about the development of optical wireless links for Intra/Extra Spacecraft and AIT scenarios within the framework of the TOWS project, founded by ESA.

Ernesto Ciaramella is Full Professor of Telecommunications at the Istituto TeCIP, at the Scuola Superiore Sant'Anna of Pisa, since 2014. He joined Scuola Superiore Sant'Anna, as Associate Professor in 2002. His research interests include various areas of optical communications (components, systems, networks). His main research contributions are related to devices for the regeneration of the optical signal, design of WDM systems for transport networks and access, and free-space optical systems (optical wireless). He is author or co-author of about 250 publications and holds 25 international patents. He participated in several European research projects. He has been coordinator of the EU-FP7 project COCONUT (2012–2015), and is now principal investigator of ESA- TOWS project, about optical wireless systems